Trim33 is essential for macrophage and neutrophil mobilization to developmental or inflammatory cues

Doris Lou Demy, Muriel Tauzin, Mylene Lancino, Véronique Le Cabec, Michael Redd, Emi Murayama, Isabelle Maridonneau-Parini, Nikolaus Trede, Philippe Herbomel

© 2017. Published by The Company of Biologists Ltd | Journal of Cell Science (2017) 130, 2797-2807 doi:10.1242/jcs.203471

RESEARCH ARTICLE

Trim33 is essential for macrophage and neutrophil mobilization to developmental or inflammatory cues

Doris Lou Demy[1,2,*], Muriel Tauzin[1,2,‡], Mylène Lancino[1,2], Véronique Le Cabec[3,4], Michael Redd[5], Emi Murayama[1,2], Isabelle Maridonneau-Parini[3,4], Nikolaus Trede[5] and Philippe Herbomel[1,2,§]

ABSTRACT

Macrophages infiltrate and establish in developing organs from an early stage, often before these have become vascularized. Similarly, leukocytes, in general, can quickly migrate through tissues to any site of wounding. This unique capacity is rooted in their characteristic amoeboid motility, the genetic basis of which is poorly understood. Trim33 (also known as Tif1-γ), a nuclear protein that associates with specific DNA-binding transcription factors to modulate gene expression, has been found to be mainly involved in hematopoiesis and gene regulation mediated by TGF-β. Here, we have discovered that in Trim33-deficient zebrafish embryos, primitive macrophages are unable to colonize the central nervous system to become microglia. Moreover, both macrophages and neutrophils of Trim33-deficient embryos display a reduced basal mobility within interstitial tissues, and a profound lack of a response to inflammatory recruitment signals, including local bacterial infections. Correlatively, Trim33-deficient mouse bone marrow-derived macrophages display a strongly reduced three-dimensional amoeboid mobility in fibrous collagen gels. The transcriptional regulator Trim33 is thus revealed as being essential for the navigation of macrophages and neutrophils towards developmental or inflammatory cues within vertebrate tissues.

KEY WORDS: Trim33, Tif1-γ, Macrophage, Neutrophil, Leukocyte recruitment, Amoeboid motility, Zebrafish

INTRODUCTION

Tissue-resident macrophages constitute 1–5% of all cells in nearly every organ of vertebrate organisms, and play important roles in tissue homeostasis and immune responses. Following early pioneer studies (Takahashi et al., 1989, 1996; Sorokin et al., 1992; Cuadros et al., 1992, 1993), it has been recently demonstrated that many of these tissue-resident macrophages do not arise from monocytes produced in the bone marrow, but from yolk sac-derived macrophages that colonize tissues early during development (Kierdorf et al., 2015), often before these tissues became vascularized (Ashwell, 1989; Kurz and Christ, 1998). One of the first organs to become colonized in this way in mammalian and avian embryogenesis is the central nervous system (CNS) (Sorokin et al., 1992; Cuadros et al., 1993), and at least in mammals, the resulting resident macrophages then comprise the microglia for the whole life of the animal (Kierdorf et al., 2015). The molecular and cellular determinants of this early colonization are mostly unknown. In the zebrafish embryo, primitive macrophages born in the yolk sac colonize the tissues of the embryo, notably the head, brain and retina, in a pattern very similar to that seen in mammalian and avian embryos (Herbomel et al., 2001). The M-CSF/CSF-1 receptor (CSF1-R) was found to be dispensable for the differentiation of these primitive macrophages in the yolk sac, but essential for their invasion into the tissues of the embryo (Herbomel et al., 2001).

To uncover more determinants of macrophage deployment in developing tissues and organs, we performed a forward genetic screen to identify new genes required for the establishment of microglia in zebrafish larvae. One of them turned out to be *trim33*. Trim33, previously known as transcriptional intermediary factor 1γ (Tif1-γ), is a nuclear protein endowed with ubiquitin ligase activity, that does not directly bind to DNA but regulates gene transcription by associating with various DNA-binding transcription factors, such as SMADs, PU.1 (also known as Spi1) and Scl (also known as Tal1) (Xi et al., 2011; Hesling et al., 2011; Bai et al., 2010; Kusy et al., 2011; Ferri et al., 2015). Trim33 has notably been implicated in TGF-β-mediated regulation of gene expression (Xi et al., 2011; Hesling et al., 2011), erythropoiesis (Ransom et al., 2004; He et al., 2006; Bai et al., 2010), the long-term fate of hematopoietic stem cells (Kusy et al., 2011; Quere et al., 2014) and epithelial mesenchymal transitions (Hesling et al., 2011, 2013), and is considered a tumour suppressor (Aucagne et al., 2011). Here, we have found that, in Trim33-deficient zebrafish embryos, primitive macrophages are unable to colonize the brain and retina to become primitive microglia. This led us to uncover a more general deficit in the migratory capacity of both macrophages and neutrophils in these mutant embryos, which affects both their constitutive amoeboid mobility in interstitial tissues and, much more severely, their ability to be recruited by any chemoattractant cues *in vivo*. Correlatively, we found that Trim33-deficient mouse bone marrow-derived macrophages (BMDMs) display a reduced amoeboid mobility in fibrous collagen gels. Thus Trim33 is revealed as a new key player in the mobility and recruitment of myeloid cells *in vivo*.

RESULTS

Moonshine mutants are devoid of primitive microglia

We used Neutral Red vital staining of primitive microglia (Herbomel et al., 2001) to screen for N-ethyl-N-nitrosourea (ENU)-generated recessive mutations that would lead to defective establishment of microglia but overall normal development. Among the mutants found in this screen, we identified NQ039MA, a mutant with no or very few Neutral Red-stained microglial cells at 3–4 days

[1]Institut Pasteur, Department of Developmental & Stem Cell Biology, 25 rue du Dr Roux, 75015 Paris, France. [2]CNRS, UMR3738, 25 rue du Dr Roux, 75015 Paris, France. [3]CNRS UMR5089, IPBS (Institut de Pharmacologie et de Biologie Structurale), 205 route de Narbonne BP64182, 31077 Toulouse, France. [4]Université de Toulouse, UPS, IPBS, 31077 Toulouse, France. [5]University of Utah, Huntsman Cancer Institute, 2000 Circle of Hope Drive, Salt Lake City, UT 94112, USA.
*Present address: Inserm UMR U1127, Institut du Cerveau et de la Moelle épinière, Campus Hospitalier Pitié Salpêtrière, 47 bd de l'hôpital, 75013 Paris, France.
‡Present address: CHU de Toulouse, Direction de la Recherche Medicale et de l'Innovation, 31059 Toulouse, France.

§Author for correspondence (philippe.herbomel@pasteur.fr)

N.T., 0000-0002-4730-391X; P.H., 0000-0002-8946-3313

Received 1 March 2017; Accepted 10 July 2017

Journal of Cell Science (2017) 130, 2797-2807 doi:10.1242/jcs.203471

post fertilization (dpf) (Fig. 1A,B,G), that also displayed an absence of circulating erythrocytes (Fig. S1A–D), as a consequence of an early apoptosis of the primitive erythroid progenitors (Fig. S1E,F). This mutant also displayed a smaller and irregularly shaped caudal fin (Fig. S1I,J, dotted line), sometimes combined with abnormalities in iridophore number and distribution (Fig. S1J′, blue arrowhead). As these non-microglial traits of the phenotype were highly reminiscent of those in the *moonshine* mutant (Ransom et al., 2004), a complementation test for the absence of circulating erythrocytes was done, which revealed that our NQ039MA mutant was indeed a new *moonshine* allele (data not shown), which we thus renamed mon^{NQ039}. Neutral Red staining of larvae homozygous for a previously published strong allele of *moonshine*, mon^{TB222} (Ransom et al., 2004) (Fig. 1C,D,G), as well as of mon^{NQ039}/mon^{TB222} larvae (Fig. 1E–G), revealed the same lack of Neutral Red-stained microglia as in mon^{NQ039} mutants. Thus, the lack of primitive microglia represents a previously unsuspected phenotypic trait of *moonshine* mutants. *Moonshine* mutations affect the *trim33* (previously called *tif1-γ*) gene. We therefore designed an anti *trim33* splice-blocking morpholino. Upon injection in one-cell stage embryos, the resulting morphants were found to display both early apoptosis of the primitive erythroid progenitors (Fig. S1G–H′) and later depletion of Neutral Red-stained microglia (Fig. 1G).

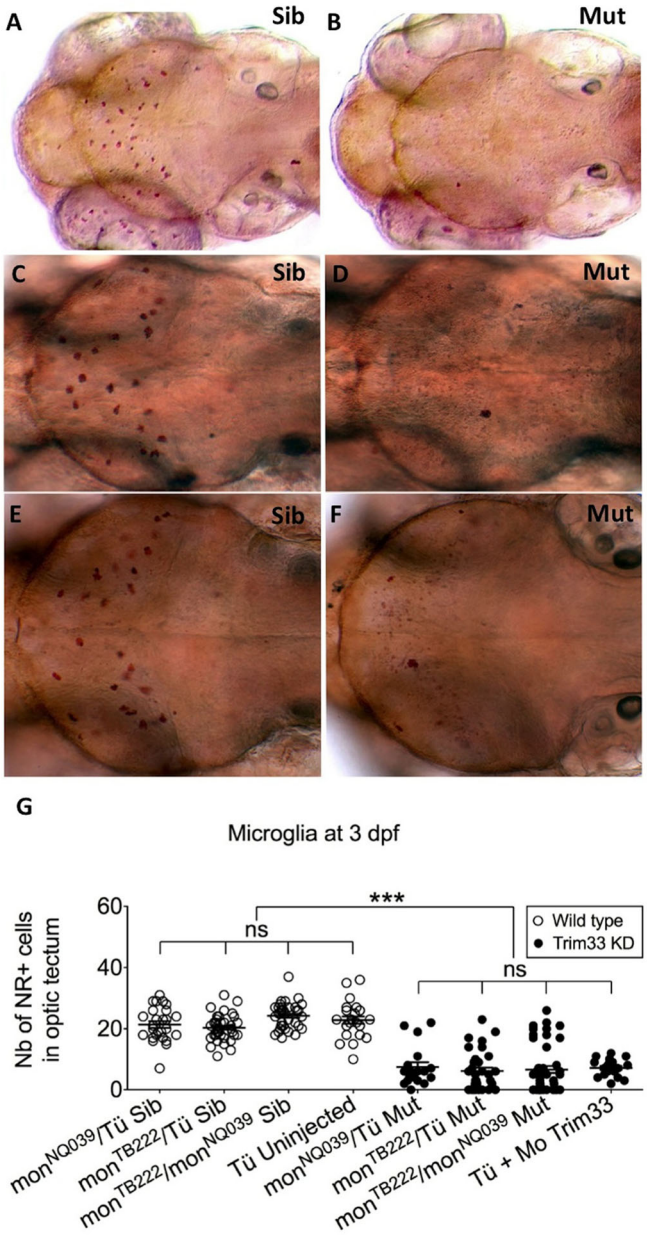

Fig. 1. *Moonshine* mutants and Trim33 morphants are devoid of microglia. (A–F) *In vivo* dorsal view of Neutral Red-stained primitive microglia in the midbrain optic tectum of 3-day-old $moonshine^{NQ039}$/*Tü* siblings (Sib) (A) and mutants (Mut) (B), $moonshine^{TB222}$/*Tü* siblings (C) and mutants (D), and of the siblings (E) and mutants (F) resulting from their complementation cross. (G) Corresponding counts (Nb, number) of Neutral Red-positive (NR+) microglial cells in the midbrain optic tectum of *moonshine* mutants and siblings, and of Trim33 morphants versus control uninjected embryos. Each dot is one embryo. Error bars show mean±s.e.m. KD, knockdown; Mo, morphant; mon, *moonshine*; Tü, wild-type Tübingen strain. ***P<0.001; ns, not significant.

Primitive macrophages are normally produced in *moonshine* mutants

Primitive microglia derive from primitive macrophages, which originate from the rostral-most lateral mesoderm of the embryo, differentiate in the yolk sac by 20–24 hours post fertilization (hpf), and spread through the interstitial tissues of the embryo within the next 12 h, and from there colonize specific epithelial tissues – the retina, brain and, more variably, the thin epidermis (Herbomel et al., 1999, 2001). To follow macrophage deployment in live embryos, we transferred the mon^{NQ039} mutation into the *Tg(mpeg1:mCherryF)* transgenic background (Nguyen-Chi et al., 2014), which highlights all macrophage populations including microglia. *In vivo* imaging revealed a globally normal number of mCherry-positive primitive macrophages throughout the embryo but with a deficit in the head by 2 dpf (Fig. 2A,D), and a lack of macrophages/microglia in the brain by 3 dpf (Fig. 2B,C; Movie 1). Whole-mount *in situ* hybridization (WISH) with a *csf1ra* probe revealed that the *csf1ra* gene, which is required for macrophage colonization of the head, including the brain and retina (Herbomel et al., 2001), is well expressed in the macrophages of *moonshine* mutants (Fig. S2A,B). It also confirmed the deficient colonization of the brain and retina by macrophages/microglia at all tested time points between 48 and 72 hpf (Fig. 2E–I). Whole-mount immunostaining for L-plastin similarly highlighted the absence of leukocytes in the brain and retina of *moonshine* mutants (Fig. S2E–G). The same was found with *trim33* morpholino injected wild-type (wt) embryos (Fig. S2C-D′ and Movie 2). Thus, in Trim33-deficient embryos, primitive macrophages are produced in normal numbers and globally spread through the embryo, but there are fewer present in the head, mostly reflecting their failure to colonize the retina and brain.

Macrophage recruitment to the retina is defective

We next investigated the features of macrophage behaviour that may lead to their lack of CNS colonization. To this aim, we focused on the retina. The retinal neuroepithelium is indeed the first epithelial tissue to become densely colonized by macrophages/microglia, and the path of this colonization is known. Macrophages begin to enter the retinal neuroepithelium by 30 hpf from its basal side, that is, from the interstitial (named 'vitreous') space between the lens and retina, which, at embryonic stages, is continuous with the rest of the cephalic mesenchyme (Herbomel et al., 2001). Hence, we studied in more detail this colonization process in both wt sibling and mutant embryos. For the live imaging of macrophages from 30 hpf, we used *Tg(pu.1:GFP)* transgenic embryos, as the *mpeg1:mCherryF* transgene was not expressed strongly enough at this early stage. Although the *pu.1:GFP* transgene is also expressed in neutrophils, which at this stage are still immature, that is they are still myelocytes

Journal of Cell Science

Journal of Cell Science (2017) 130, 2797-2807 doi:10.1242/jcs.203471

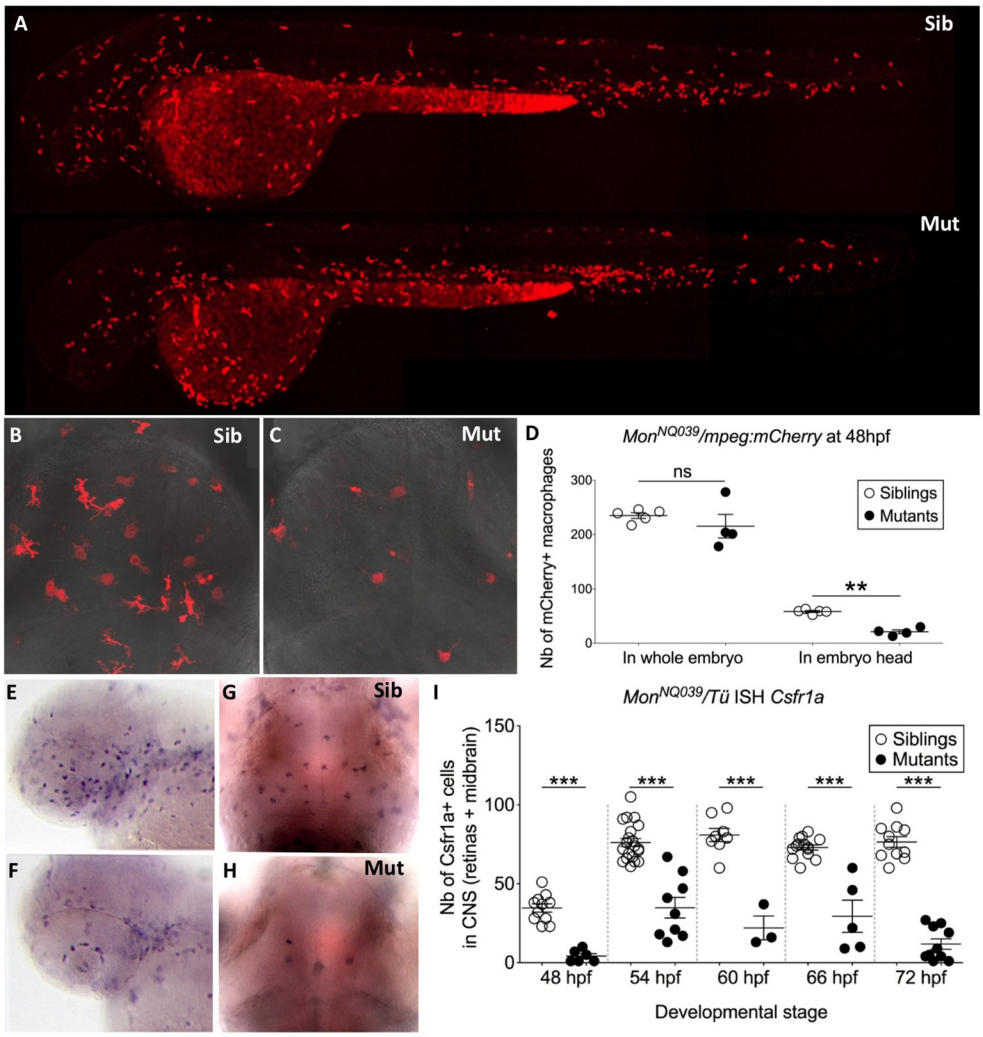

Fig. 2. Macrophages are produced normally but do not colonize the CNS in *moonshine* mutants. (A–C) *In vivo* images of whole *mon*^{NQ039}*Tg(mpeg1:mCherryF)* siblings (Sib) (A, upper) and mutants (Mut) (A, lower) at 48 hpf, and dorsal view (rostral up) of the midbrain of siblings (B) and mutants (C) at 72 hpf. (D) Counts (Nb, number) at 48 hpf show that *mon*^{NQ039}*Tg(mpeg1:mCherryF)* mutant embryos have significantly less mCherry-positive macrophages in the head despite having a similar total number of macrophages to that in the siblings. ISH, whole-mount *in situ* hybridization. (E–I) Whole mount *in situ* hybridization for *Csfr1a* mRNA reveals numerous macrophages in the retina at 48 hpf (E) and midbrain at 72 hpf (G) in the siblings, whereas very few such cells can be detected in these organs in the mutants (F,H). (I) Counting of these cells over time reveals a lower number in the mutant CNS at all stages. Error bars show mean±s.e.m. $^{**}P<0.01$; $^{***}P<0.001$; ns, not significant.

(Le Guyader et al., 2008), we know that neutrophils do not colonize the CNS in wt (Le Guyader et al., 2008) nor in *moonshine* embryos (see below). By 30 hpf, the normal onset of retina colonization, the number of *pu1:GFP*+ leukocytes that reached the eye was much lower in *mon*^{NQ039} mutants (Fig. 3B; n=6; 3.2 cells/embryo), than in wt siblings (Fig. 3A; n=6; 17.5 cells/embryo). Immunodetection and counting of L-plastin-positive leukocytes confirmed this difference, and showed in addition that by 36 hpf, the mutant had reached the number of myeloid leukocytes found at the wt eye at 30 hpf, and then plateaued at that level. In contrast, the number of leukocytes in the wt eye kept increasing, and at all stages most of them were located in the retinal parenchyma, where their number reached a plateau by 48 hpf at ∼32 cells/retina (Fig. 3C, left graph), in agreement with our previous observations (Herbomel et al., 2001). In contrast, in *moonshine* mutants, only a few macrophages were found within the retinas by 36 hpf, and their number then did not increase further (Fig. 3C, right graph). We then monitored, by time-lapse confocal imaging, the behaviour of myeloid leukocytes in and around the retina from 48 hpf onwards, and tracked their 3D trajectories (Fig. 3D,E; Movie 3). The tracking of macrophages in wt embryos revealed that most of their wandering during the 12 h imaging session occurred within the retinal tissue or from the vitreous space into the retina. In contrast, the 4D tracking of the few myeloid leukocytes found in the mutant eye revealed that most were wandering solely within the vitreous space, mostly along the retinal pial surface, and the few that entered the retina did not remain there (Fig. 3E,F; Movie 3; see also Fig. 2F). Taken together, these data point to a delayed and reduced recruitment of primitive macrophages to the eye, followed by their failure to enter the retina, in Trim33-deficient mutants.

Moonshine macrophages and neutrophils display a reduced basal mobility in interstitial tissues

Our 4D tracking statistics of myeloid cells near to the retina also revealed that mutant myeloid cells in the cephalic interstitial tissues around the eye (Fig. 3D,E, green tracks) had an almost 2-fold reduced mobility in terms of average speed compared to that seen in the siblings (Fig. 3G).

This led us to investigate the basal mobility of mutant versus sibling macrophages in a larger area of interstitial tissue, covering most of the cephalic mesenchyme posterior to the eye and part of the yolk sac. In addition, since in fish, unlike in mammals, neutrophils live and wander mostly in interstitial tissues, as do the macrophages (Le Guyader et al., 2008), we simultaneously studied the basal mobility of both cell types in a *Tg(mpeg1:mCherryF; mpx:gfp)* double transgenic background from 48 hpf onwards. First, we found that the total numbers of both cell types were normal in *moonshine* embryos (Fig. S3). So was the overall distribution of neutrophils along the body (Fig. S3D), unlike that of macrophages, which showed significant differences in the mutant, with less in the head as

Journal of Cell Science (2017) 130, 2797-2807 doi:10.1242/jcs.203471

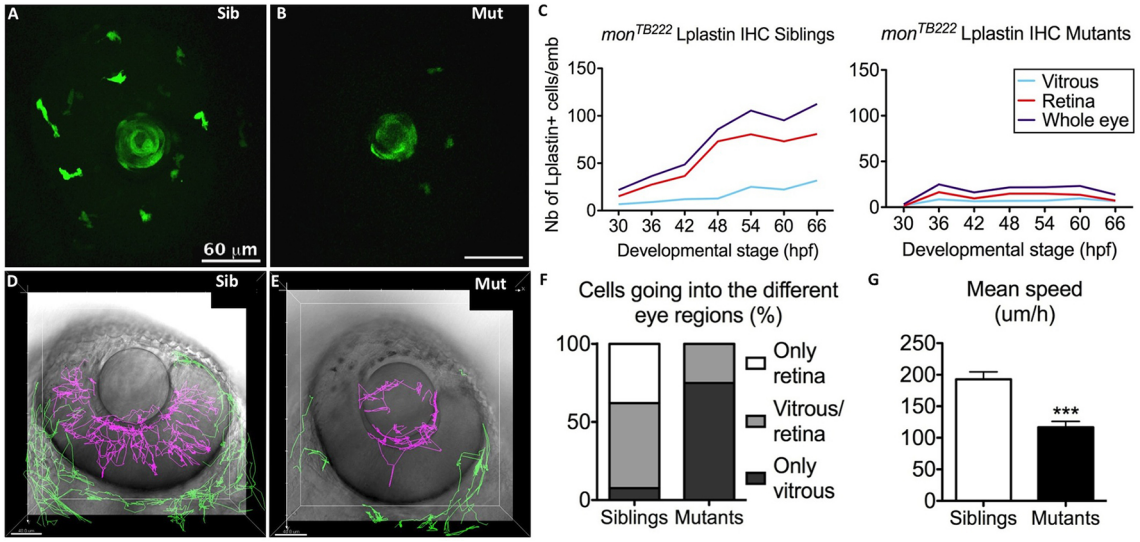

Fig. 3. *Moonshine* macrophages display a defective recruitment towards the eye and into the retina. (A,B) *In vivo* observation of *mon*^{NQ039}*Tg(Pu1:gfp)* siblings (Sib) (A) and mutants (Mut) (B) at 30 hpf reveals that several GFP-positive myeloid cells have already arrived at the eye in the siblings, whereas there are few in the mutants; the lens shows apparent green fluorescence only due to its optical properties. (C) Counts (Nb, number) of L-plastin-positive leukocytes in the retina (red curve) and in the vitreous space (from where wt macrophages enter the retina; light blue curve) of *mon*^{TB222}*/Tü* siblings (left graph, 10–18 embryos/timepoint) and mutants (right graph, 10–16 embryos/timepoint) show an increasing number of macrophages in the eye (blue curve) and resulting colonization of the retina (red curve) in the sibling, whereas very few macrophages arrive at the eye in the mutants and their number does not increase with time. IHC, immunohistochemistry. (D–G) 4D tracking for 12 h of GFP-positive myeloid cells inside (pink tracks) and outside (green tracks) the eye in *mon*^{NQ039}*Tg(Pu1:gfp)* siblings (D) and mutants (E) from 48 hpf showing that the few mutant cells inside the eye mostly do not invade the retina (*n*=20 cells from two embryos), whereas it is the opposite in the siblings (*n*=66 cells from two embryos), as quantified in F. (G) Myeloid cells in the mesenchyme peripheral to the eye (green tracks) migrate more slowly in the mutants (*n*=42 cells from two embryos, mean speed 116.7 µm/h) than in the siblings (*n*=109 cells from two embryos, mean speed 192.9 µm/h). Error bars show the s.e.m. ***P<0.001.

mentioned previously, and more in the yolk sac, their site of origin (Fig. S3E). Locally, macrophages and neutrophils often appeared more clustered, closer to one another, than in wt embryos (Fig. 4A,B). Time-lapse imaging then showed that both macrophages and neutrophils had a clearly reduced basal mobility in mutant embryos (Movie 4). This was analysed quantitatively subsequent to their 4D tracking. Macrophages and neutrophils in wt embryos migrate very efficiently and in complementary ways, macrophages being slower but covering the whole area more extensively than neutrophils (see colour-coded speed in Fig. 4A′,A″), which appear to move faster and along preferential routes. The same analysis applied to mutants showed that both macrophages (Fig. 4B′) and neutrophils (Fig. 4B″) migrate less than in wt sibling embryos (smaller covered area for similar numbers of analysed cells, Fig. 4C). Quantification of the mean square displacement over time confirmed that both myeloid cell types explore much less space in the mutant (Fig. 4D,E). Thus, *moonshine* mutants display a general defect in the basal mobility of macrophages and neutrophils in interstitial tissues.

Macrophages and neutrophils fail to be recruited to inflammatory signals in *moonshine* larvae

We then assessed whether strong inflammatory recruitment signals would be able to attract the macrophages and neutrophils in mutant larvae as they normally do in wt. To test this, we performed time-lapse imaging of the *in vivo* behaviour of macrophages and neutrophils in three types of situations: upon tail tip transection, upon leukotriene B4 (LTB4) bath treatment (Yoo et al., 2011), and upon bacteria injection in the inner ear (Le Guyader et al., 2008). Wounding or bacterial injections should recruit macrophages and neutrophils, while LTB4 bath treatment should attract neutrophils.

Caudal fin tip transection at 3 dpf caused a recruitment and accumulation of both macrophages (mCherry-positive) and neutrophils (GFP-positive) at the wound in wt (Fig. 5A, *n*=6), but not in *moonshine* mutant, larvae (Fig. 5B, *n*=6). Cell counts performed every hour after wounding (Fig. 5C) showed the progressive recruitment of both macrophages (red triangles) and neutrophils (green triangles), with the number of neutrophils and of macrophages at the wound plateauing at 6 h and 9–12 h post wounding (pw), respectively. In mutant larvae (Fig. 5C, red and green circles), very few macrophages or neutrophils were recruited to the wound, and their number no longer increased after 3 h pw. We further asked whether these few mutant leukocytes found at the wound had been recruited with the same efficiency as the wt ones. The 4D tracking of all cells recruited during the first 3 h pw (Fig. 5A′,A″,B′,B″; Movie 5) and subsequent quantitative analysis of their trajectories (Fig. S4) revealed that in wt larvae, recruited neutrophils migrated at higher speed (370.5 µm/h) than macrophages (156.7 µm/h), but with similar track straightness (0.8 vs 0.75). In contrast, the very few neutrophils and macrophages recruited in the mutant larvae both migrated at a mean speed three times lower than their wt counterparts (neutrophils, 126.5 µm/h; macrophages, 52.5 µm/h; Fig. S4) and trajectories towards the wound were not so straight (neutrophils, 0.57 vs 0.8; macrophages, 0.35 vs 0.75; Fig. S4).

An equally severe neutrophil recruitment defect was observed in *mon*^{NQ039} larvae upon addition of 30 nM LTB4 to the medium bathing 3 dpf larvae. Mutant and sibling larvae were subjected to time-lapse imaging in parallel in the same dish, and LTB4 was added to their common bath during the imaging session. As can be seen in Fig. 5D–F and in Movie 6, for the wt larvae, LTB4 addition to the embryo medium at time step 13 of the time-lapse sequence induced, within minutes, a strong recruitment of neutrophils from the caudal hematopoietic tissue (CHT) (Murayama et al., 2006), a stromal space between the caudal artery and vein, towards more superficial locations underneath the skin overlying the somite

Journal of Cell Science (2017) 130, 2797-2807 doi:10.1242/jcs.203471

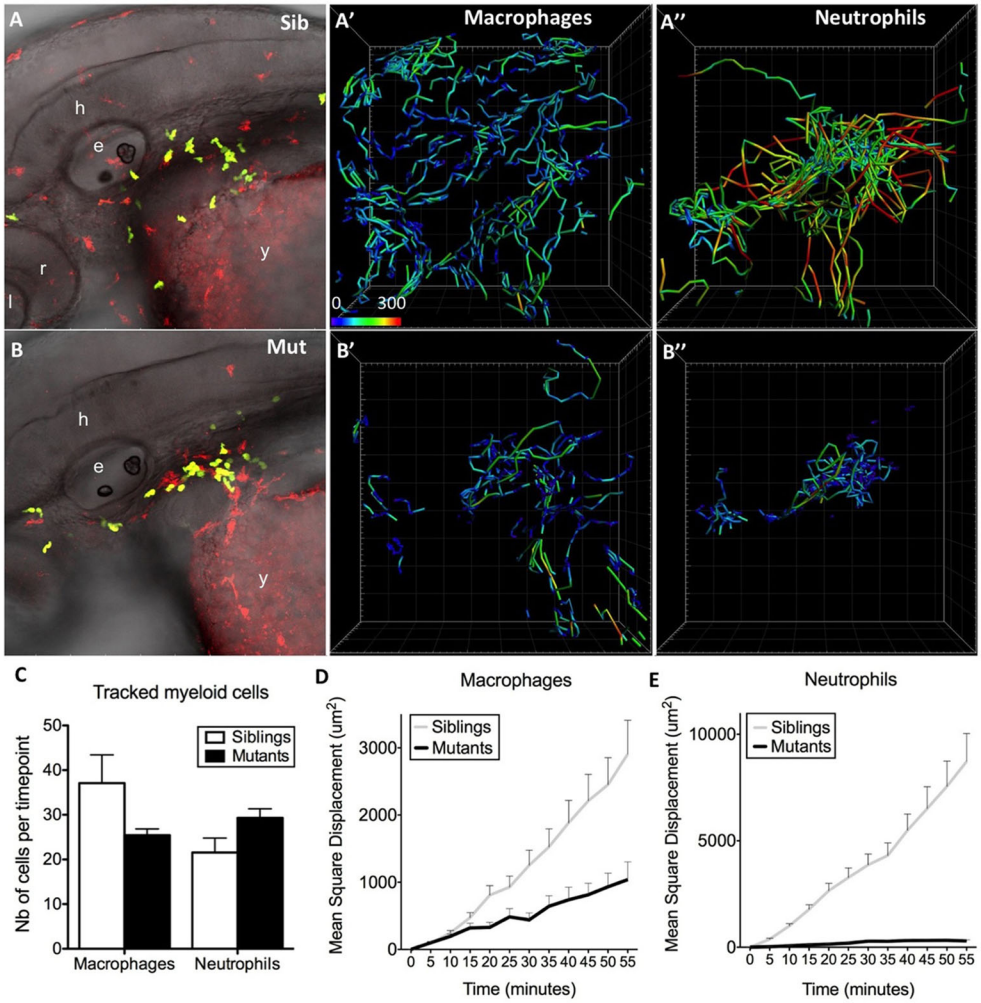

Fig. 4. The basal migration in interstitial tissues of both macrophages and neutrophils is affected in *moonshine* mutants. *In vivo* 4D tracking of mCherry-positive macrophages and GFP-positive neutrophils in the head and anterior yolk sac area of *mon*^{NQ039}*Tg(mpeg1:mCherryF; mpx:gfp)* sibling (Sib) (A–A″) and mutant (Mut) (B–B″) embryos at 48 hpf. e, ear; l, lens; y, yolk sac; h, hindbrain; r, retina. Cell trajectories are shown in panels (A′,A″,B′,B″), with colour coding of speed (from 0 to 300 µm/h), and the number (Nb) of cells tracked per time point in each case is shown in C (as mean±s.d. for 80 time points). (D,E) Quantification of the mean±s.d. square displacement over time illustrates the migration defect of the mutant leukocytes.

muscles and the ventral fin (Fig. S5; Fig. 5D, green channel; Fig. 5F, grey curve; Movie 6, left panel). In contrast, neutrophils in the CHT of the *mon*^{NQ039} mutant did not react to LTB4 addition within 2.5 h of imaging (Fig. 5E, green channel; Fig. 5F, black curve; Movie 6, right panel).

Finally, as bacterial infection is considered the strongest attractive signal for innate immune cells, we turned to bacterial injections in the inner ear (otic vesicle) to try and recruit myeloid cells in the *moonshine* mutant. *E. coli* injection in the ear of *mon*^{NQ039} *Tg(mpeg1:mCherryF; mpx:gfp)* larvae at 3 dpf induced, within minutes, a strong recruitment of macrophages (Fig. 6A,B; Movie 7, left panel) and neutrophils (Fig. 6C,D; Movie 7, left panel) towards and then into the ear for the sibling larvae, whereas in *mon* mutants, none or very few of either myeloid cell type were recruited to the infection site within 7 h of observation (Fig. 6E–H; Movie 7, right panel).

Aside from these gram-negative bacteria, we also injected gram-positive GFP-expressing *B. subtilis* bacteria in the ear of *mon*^{NQ039} *Tg (LysC:DsRed)* embryos, which highlight neutrophils in red (Movie 8). Again, while neutrophils were quickly and massively recruited to the infected ear of the sibling larvae, they were not recruited in the mutant larvae. We quantified whether the ear infection caused any sign of reaction of the neutrophils in the mutant larva by measuring their distance to the infected ear over time. As can be seen in Fig. 6I, in less than 2 h post-infection of a wt larva, the mean distance of neutrophils in the field of view (the whole head) to the infected ear dropped from ∼100 µm to half of that (grey curve); in contrast, no significant change was found over 6 h of follow-up in the mutant (black curve). Similarly, the number of neutrophils inside the otic vesicle kept increasing over time in the infected sibling (Fig. 6J, grey curve), but not in the mutant (Fig. 6J, black curve).

The defect in basal neutrophil mobility in *moonshine* mutants is cell autonomous

The various migration defects displayed by myeloid cells in mutant embryos both at steady state and when recruited to different locations, at different stages and by different attractive signals, suggest that the mutation affects these cells in an autonomous manner. In order to confirm this, we took advantage of a convenient technique recently developed in our lab to obtain partially fused parabiotic embryos of any two genetic backgrounds (Demy et al., 2013). Here, we fused wt *Tg(Mpx:GFP)* embryos with mutant *Tg (LysC:DsRed)* embryos, and tracked the basal mobility within interstitial tissues of both the red and green neutrophils in both the wt and the mutant parabiont. As can be seen in Fig. 7 and Movie 9, the neutrophils trans-colonized both parabionts, allowing us to track the neutrophils from both backgrounds in both parabionts (Fig. 7). In a 3 h cell tracking, we found a non-significant difference between the mean speed of wt neutrophils in the wt embryo (331.2 µm/h) and in the mutant embryo (284.7 µm/h), indicating that the mutant environment does not affect the basal mobility of wt neutrophils. In contrast, the mobility of mutant neutrophils was very significantly affected both in the mutant (143.2 µm/h) and in the wt (174.5 µm/h)

Journal of Cell Science (2017) 130, 2797-2807 doi:10.1242/jcs.203471

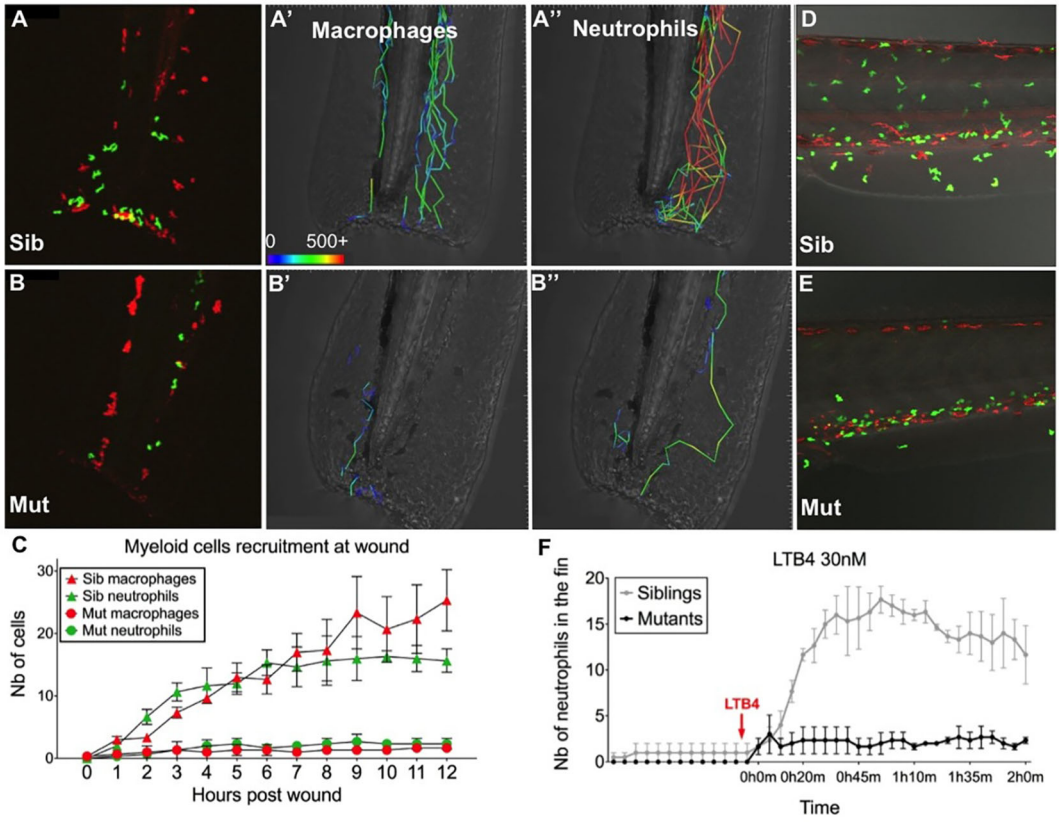

Fig. 5. *Moonshine* mutant myeloid cells do not respond to attractive signals. (A–E) *In vivo* confocal time-lapse imaging of the caudal fin (A–B″) or CHT region (D,E) of 3-day-old *mon*^{NQ039}*Tg(mpeg1:mCherry;mpx:gfp)* siblings (Sib) (A–A″,D) and mutants (Mut) (B–B″,E); macrophages are red, neutrophils are green. (A–B″) Fluorescence images at 9 h post tail fin tip transection (9 hpw) (A,B) and trajectories of the first recruited cells, from 0 to 3 hpw (A′–B″); cell speeds (in µm/h) are colour coded as indicated by the bar in A′; cell speeds ≥500 µm/h are all coded in red. (C) Macrophage and neutrophils counts (Nb, number) at the wound over time (mean±s.e.m.; *n*=3 sibling and 3 mutant larvae). (D–F) LTB4 addition experiment. (D,E) Images at 1.5 h post LTB4 addition, showing the recruitment of neutrophils from the CHT to the ventral fin and skin in the sibling (D), but not in the mutant (E). (F) Neutrophil counts in the ventral fin during the time-lapse sequence (*n*=3 experiments).

parabionts, indicating that Trim33 deficiency affects the basal motility of neutrophils in interstitial tissues in a cell-autonomous manner.

Trim33-deficient mouse macrophages are impaired in their amoeboid motility

To assess whether such a role of Trim33 would be conserved in mammals, we took advantage of the recent availability of mice harbouring *Trim33* gene disruption specifically in myeloid leukocytes (Ferri et al., 2015). We derived macrophages from the bone marrow of these or control mice, and quantified their M-CSF-dependent mobility *in vitro* in a 3D-fibrous collagen gel, which triggers macrophage amoeboid (protease-independent) mobility, or in Matrigel, which triggers a 'mesenchymal' (protease-dependent) mode of macrophage migration (Van Goethem et al., 2010). We found that TRIM33-deficient BMDMs have a clearly reduced migration capacity in a fibrous collagen gel (Fig. 8A). Interestingly, their migration capacity in Matrigel was not or was only barely affected (Fig. 8B). Consistent with the latter result, TRIM33-deficient BMDMs were not detectably affected in their ability to form podosome rosettes (Fig. 8C), which correlate with macrophage migration capacity in Matrigel, but not in fibrous collagen gels (Cougoule et al., 2010; Van Goethem et al., 2011). Thus, TRIM33 deficiency substantially hinders the 3D amoeboid mobility of mouse BMDMs, as it does *in vivo* for primitive macrophages in Trim33-deficient zebrafish embryos.

DISCUSSION

We have found that in Trim33-deficient zebrafish embryos, macrophages are unable to colonize the brain and retina to become microglia, and that macrophages and neutrophils display a reduced basal mobility in interstitial tissues, and a profound unresponsiveness to inflammatory recruitment cues, including the strongest known – local bacterial infections. These migration defects are unlikely to be caused by the lack of circulating erythrocytes in *moonshine* mutants. In the small zebrafish embryo, oxygen is indeed supplied by diffusion from the water through the very thin skin. Convective transport of oxygen by circulating erythrocytes begins to contribute to tissue oxygenation only much later – by 12–14 dpf (Rombough, 2002). Correlatively, preventing blood circulation from its onset does not compromise the microglial colonization of the brain (Xu et al., 2016). Finally, our cell autonomy experiments confirmed that *trim33* mutant neutrophils are unable to properly migrate even within a wt embryo, in the presence of circulating wt erythrocytes.

To fully appreciate the significance of our findings, it may be useful to recall the anatomical context in which these leukocyte migrations occur. In zebrafish embryos and early larvae, primitive macrophages and neutrophils are both born in the yolk sac interstitium, from where they invade the interstitial mesenchyme of the embryo, where many then reside and keep wandering. From this space, the only epithelial organs colonized by these cells are the brain and retina, by macrophages only, and in a variable manner the monolayered epidermis, by macrophages and neutrophils

Journal of Cell Science (2017) 130, 2797-2807 doi:10.1242/jcs.203471

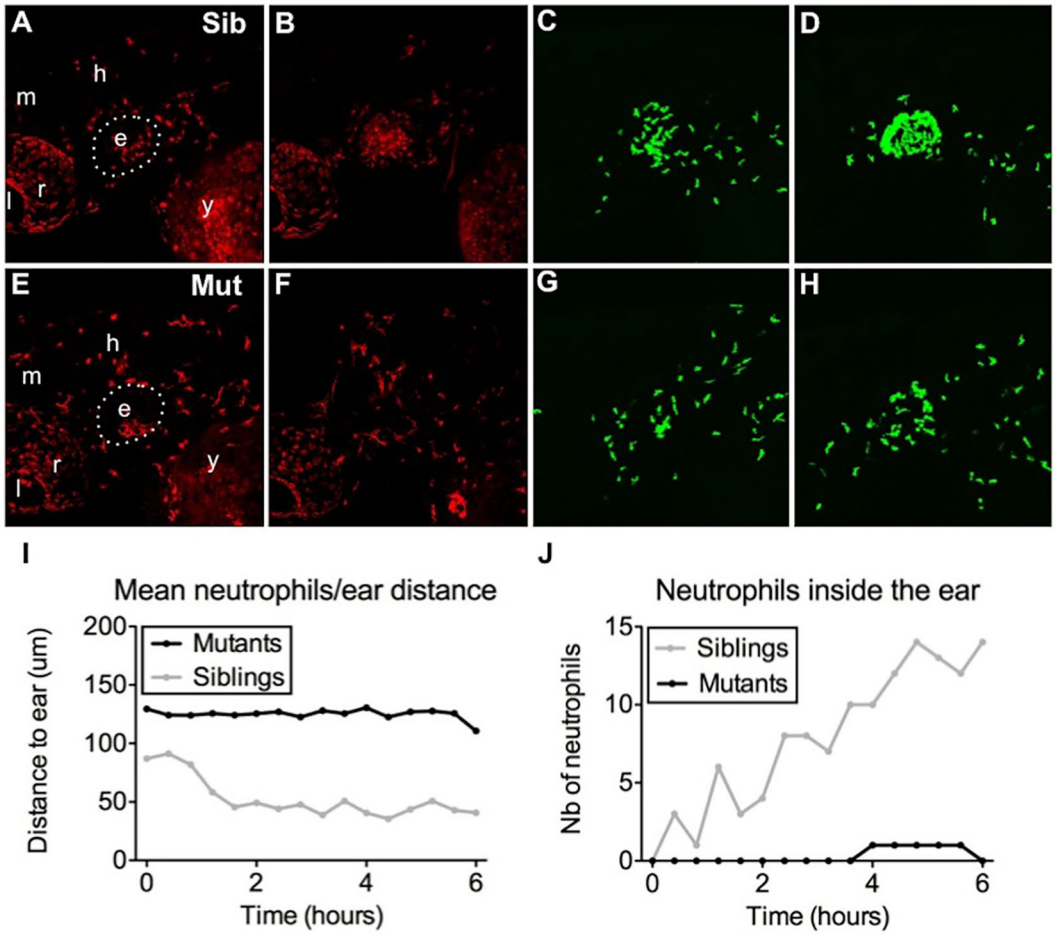

Fig. 6. Bacterial infection is insufficient to recruit mutant myeloid cells. (A–H) *In vivo* time-lapse imaging of macrophages (A,B,E,F) and neutrophils (C,D,G,H) of *mon*^{NQ039}*Tg(mpeg1:mCherry/mpx:gfp)* sibling (Sib) (A–D) and mutants (Mut) (E–H) by 60 hpf, 20 min after *E. coli* injection in the inner ear (A,C,E,G) or 7 h later (B,D,F,H). Bacteria injection in the ear induces a strong recruitment of both macrophages and neutrophils in the siblings (B,D), but almost none in the *moonshine* mutant (F,H). e, ear; l, lens; r, retina; m, midbrain; h, hindbrain; y, yolk sac. See also Movie 7. (I,J) Quantification of neutrophil mean distance to the ear following injection of GFP-positive *B. subtilis* in the inner ear by 72 hpf (I) shows a drop during the first 2 hours post injection in the siblings (light curve) and not in the mutant (black curve); accordingly, the number of neutrophils inside the ear of infected larvae constantly increases over time in the siblings (light curve) but not in the mutant (black curve). See also Movie 8.

(Herbomel et al., 2001; Le Guyader et al., 2008). Therefore the differential migration behaviours explored in the present work do not concern extravasation from blood vessels, but migration within the interstitial mesenchyme, and from there penetration of the retina and brain (and otic vesicle in the ear infection experiments). We found that the lack of retina colonization by macrophages in the mutant resulted from a delayed and reduced presence of macrophages in the eye area, followed by their inability to invade the retinal parenchyme. Since the developmental migration of primitive macrophages from the yolk sac into the head is fully dependent on the M-CSF/CSF-1 receptor (Herbomel et al., 2001), our data firstly suggest that Trim33-deficient primitive macrophages display a delayed and weaker response to chemoattractant CSF1-R ligands (Mouchemore and Pixley, 2012; Lelli et al., 2013). In addition, the inability of the few mutant macrophages that reached the eye to penetrate and stay in the retina could reflect an unresponsiveness to the same or different (still uncharacterized) chemoattractants expressed by the retina, or it may reflect a decreased capacity of the mutant macrophages to invade epithelial tissues. In any case, a defective response of mutant macrophages to MCSF-R chemoattractant ligands, together with their profound insensitivity to inflammatory cues, would emphasize the pervasiveness of their navigation deficiency, as CSF1-R is a receptor tyrosine kinase (RTK), while receptors involved in recruitment to wounds and infections are predominantly G-protein-coupled receptors (GPCRs). To our knowledge, Trim33 deficiency is the first genetic defect found to lead to such a pervasive lack of response from both macrophages and neutrophils to both developmental and inflammatory chemoattractants *in vivo*. Interestingly, the early chemokine-dependent colonization of the thymus rudiment by lymphoid progenitors (Hess and Boehm, 2012) is not affected in Trim33-deficient mutants (Ransom et al., 2004; Monteiro et al., 2011), suggesting that the navigation defect is restricted to leukocytes of the myeloid family. Macrophages then neutrophils (in this order) are the most PU.1-dependent leukocyte cell types. In mammals, TRIM33 was found able to interact physically with PU.1, co-bind with it to hematopoietic gene regulatory elements (Kusy et al., 2011), and more recently, to regulate the transcriptional response of the interferon-β gene specifically in macrophages in a PU.1-dependent manner (Ferri et al., 2015). We therefore surmise that the profound navigation defect shown by macrophages and neutrophils in Trim33-deficient developing zebrafish likely reflects the mis-regulation in these cells of genes co-regulated by Pu.1 and Trim33. It could be one gene

Journal of Cell Science (2017) 130, 2797-2807 doi:10.1242/jcs.203471

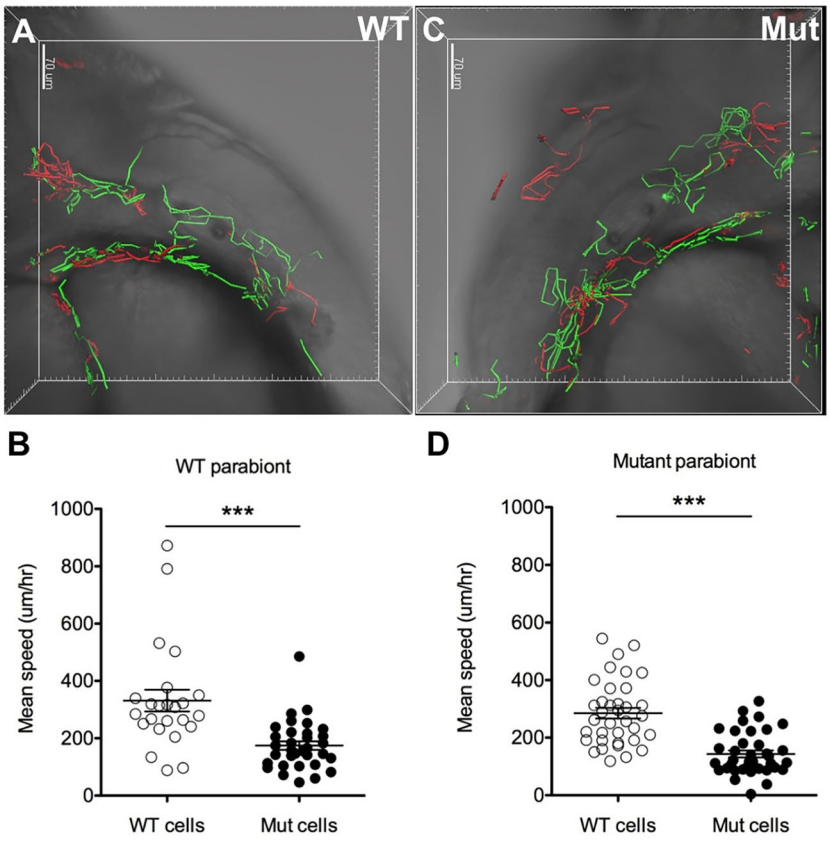

Fig. 7. The defect in neutrophil basal migration in *moonshine* mutants is cell-autonomous. 4D tracking of wild-type (WT) GFP-positive (green tracks) and mutant DsRed-positive (red tracks) neutrophil mobility within interstitial tissues during 3 h of parallel confocal imaging of one wild-type (A) and one mutant (Mut) (C) parabiotic embryos (fused at the level of the trunk) at 48 hpf shows a significantly diminished mobility (average speed; error bars show mean±s.e.m.) of the mutant cells both in the wild-type (B) and in the mutant (D) parabionts, whereas the migration of wild-type neutrophils is not affected in the mutant parabiont (D), together indicating that the mutant neutrophil phenotype is cell autonomous. ***P<0.001. See also Movie 9.

encoding a still undiscovered key effector of amoeboid cell navigation, or a whole network of known and unknown effectors, in which case Trim33 would be a master regulator of myeloid cell navigation.

It remains to be investigated whether such profound mobilization defects also occur in myeloid cells produced in adult hematopoietic organs. Importantly, our data already show that the role of Trim33 in amoeboid motility is conserved in adult mouse BMDMs.

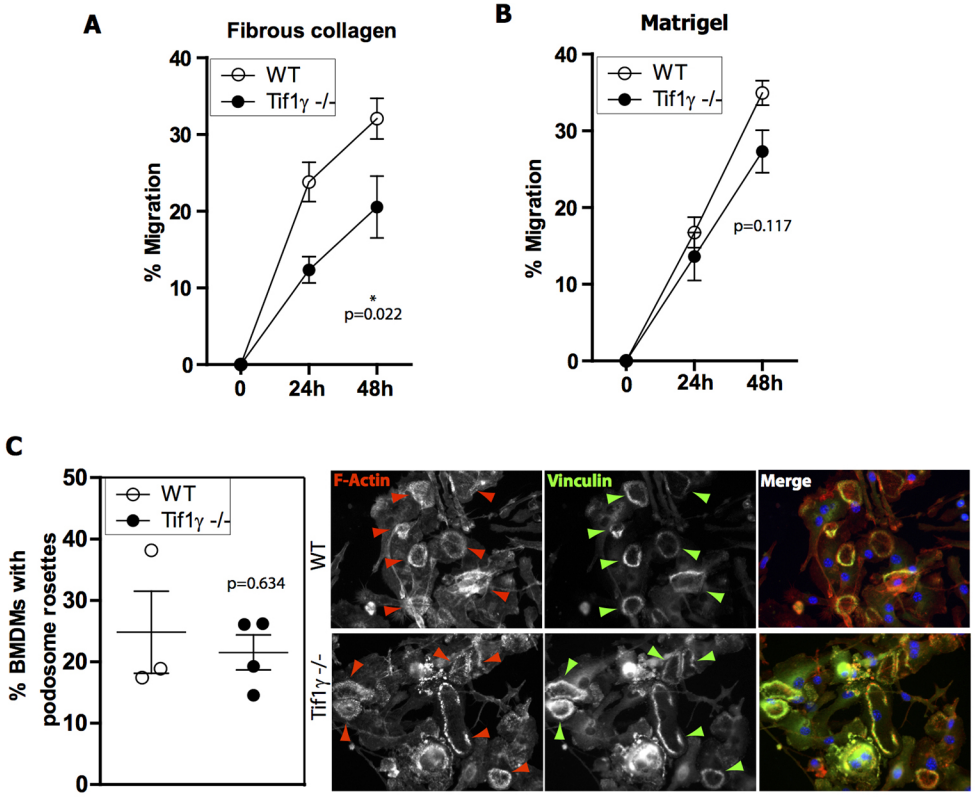

Fig. 8. Trim33-deficient mouse BMDMs are impaired in their amoeboid migration capacity. (A,B) ~500 WT BMDMs (open circles) or *Trim33*$^{-/-}$ (Tif1γ -/-; black circles) BMDMs per mouse were loaded on the top of thick layers of fibrous collagen (A) or Matrigel (B) polymerized in transwell inserts. The percentage of cells that migrated into the matrix was monitored at 24 and 48 h. Results are expressed as mean±s.e.m. of macrophages from four mice. *P*-values were obtained with two-way ANOVA with Bonferroni's post-test. (C) WT BMDMs (open circles) or *Trim33*$^{-/-}$ (black circles) BMDMs adherent on glass coverslips for 24 h were fixed and stained with DAPI (blue), F-actin (phalloidin conjugated to Texas Red) and vinculin (green). Arrows indicate podosome rosettes. The percentage of BMDMs with podosome rosettes was quantified (mean±s.e.m. of three to four mice). *P*-values were obtained with an unpaired two-tailed Student's *t*-test.

Journal of Cell Science

Journal of Cell Science (2017) 130, 2797-2807 doi:10.1242/jcs.203471

Thus, Trim33, so far known for its role in erythropoiesis, adult hematopoietic stem cell potential, and TGFß signalling, is revealed here to be a key factor in a new area, the amoeboid motility of myeloid leukocytes *in vivo* and their ability to respond to any developmental or inflammatory cues. A future analysis of gene networks regulated by Trim33 in myeloid cells should lead to new insights in the genetic requirements for leukocyte amoeboid motility and recruitment.

MATERIALS AND METHODS

Zebrafish

Wild-type, transgenic and mutant zebrafish embryos were raised at 28°C in embryo water [Volvic™ water containing 0.28 mg/ml Methylene Blue (M-4159; Sigma) and 0.03 mg/ml 1-phenyl-2-thiourea (P-7629; Sigma) to prevent melanin formation].

Tübingen (Tü) wild-type fish, and the transgenic lines *Tg(mpeg1:mCherryF)* (Nguyen-Chi et al., 2014), *Tg[(tbp:Gal4)^{f13};(UAS:SEC-Hsa.ANXA5-YFP;myl7:RFP)^{f12}]* (van Ham et al., 2010), *Tg(mpeg1:Gal4FF)^{gl25}* (Palha et al., 2013), *Tg(mpx:GFP)^{i114}* (Renshaw et al., 2006), *Tg(pu.1:GFP)^{df5}* (Hsu et al., 2004), *Tg(gata1:dsRed)^{sd2}* (Traver et al., 2003), *Tg(lyz:DsRed2)^{nz50}* (Hall et al., 2012) have been used in this study. The *moonshine^{NQ039MA}* mutant was obtained by N-ethyl-N-nitrosourea (ENU) chemical mutagenesis on a Tü wild-type background, within the Tübingen 2005 Screen as part of the FP6 European Integrated Project 'Zebrafish models for human development and disease'. Briefly, founder wild-type males were exposed to ENU and subsequently outcrossed to raise F1 and F2 families as described previously (van Eeden et al., 1999). F3 larvae were screened at 4 dpf for specific defects in Neutral Red-stained microglia but no apparent morphological defects. Mutant NQ039MA was thus recovered, and identified as a new allele of *moonshine* through its non complementation of *moonshine^{tb222}* (Ransom et al., 2004). Both *moonshine* alleles were then maintained on a Tü genetic background.

Zebrafish husbandry was performed according to approved guidelines.

Neutral Red vital staining of microglia

Microglial cells were revealed in 3-day-old live larvae by adding the Neutral Red vital dye (N-4638; Sigma) to the embryo water at a final concentration of 5 mg/ml. Larvae were then incubated in the dark at 28°C for 1.5–2 h, rinsed, anesthetized and observed under a stereomicroscope.

O-dianisidine staining of erythrocytes

For histochemical staining of haemoglobin, deeply anesthetized embryos and larvae were placed in freshly prepared *o*-dianisidine solution [40% ethanol with 0.01 M sodium acetate, 0.65% H_2O_2, and 0.6 mg/ml *o*-dianisidine (D-9143; Sigma) for 10 (>5 dpf), 15 (4 dpf), 20 (3 dpf), 30 (48 hpf) or 45 (24 hpf) min, then washed in PBT, and fixed in 4% methanol-free formaldehyde (4018; Polysciences)].

Bodipy ceramide vital staining of tissues

Bodipy ceramide (D-3521; Molecular Probes) was dissolved in dimethyl sulfoxide (DMSO) at a concentration of 5 mM for stock solution. Dechorionated live embryos were soaked in 5 µM bodipy ceramide solution overnight in the dark, then washed five times with Volvic water and mounted in 1% low-melting-point agarose for confocal fluorescence microscopy.

Whole-mount *in situ* hybridization and immunohistochemistry

Whole-mount *in situ* hybridization (WISH) was performed according to Thisse and Thisse (2008) on embryos fixed every 6 h from 48 hpf to 72 hpf.

Whole-mount immunohistochemistry was performed as described previously (Murayama et al., 2006), omitting the acetone treatment, using rabbit anti-zebrafish L-plastin polyclonal antibodies (Le Guyader et al., 2008), followed by Cy3-coupled secondary anti-rabbit antibody (111-166-003; Jackson Immunoresearch) at 1:800 dilution.

Morpholino injections

A splice-blocking antisense morpholino against the *trim33* exon1–intron1 donor splice junction was synthesized by Gene Tools (5′-CTTCCCCTTTCCGAACTTACCGATT-3′), and 3–5 nl of 1 mM MO solution was microinjected in one- to two-cell-stage embryos.

In vivo microscopy and image analysis

Video-enhanced differential interference contrast and fluorescence wide-field microscopy were performed as described previously (Herbomel and Levraud, 2005), through the 40×1.00 NA water-immersion objective of a Nikon 90i microscope. Resulting images were collected using BTVpro software (Bensoftware, London).

For time-lapse confocal fluorescence imaging, embryos and larvae were mounted in 1% low-melting-point agarose (V-2111; Promega) dissolved in embryo water, and supplemented with 0.16 mg/ml tricaine (A-5040; Sigma) for fluorescence time-lapse imaging. After solidification, embryo medium with 0.16 mg/ml tricaine solution was added in order to keep embryos hydrated during experiments. Thereafter, images were captured at the selected times on an inverted Leica SP8 set-up allowing multiple point acquisition, so as to image mutants and their siblings in parallel.

Image stacks from confocal imaging were processed with LAS software to generate maximum intensity projections or were exported into Imaris software (Bitplane) for 3D tracking of macrophage and neutrophil trajectories.

Inflammatory recruitment assays

For the tail wound assay, larvae were anesthetized in embryo water supplemented with 0.16 mg/ml tricaine, and complete transection of the tailfin tip was performed with a disposable sterile scalpel. Larvae were then mounted and imaged for confocal time-lapse microscopy.

The LTB4 (L-0517; Sigma) bath assay was performed as described previously (Yoo et al., 2011). In order to capture time-points before and after LTB4 addition, LTB4 was added directly to the embryo medium at a final concentration of 30 nM during the time-lapse imaging of a mutant and a sibling larvae mounted and imaged in parallel in the same dish.

For bacteria injection assays, *E. coli* bacteria expressing CFP or *B. subtilis* expressing GFP were grown in LB broth, prepared and injected in the otic cavity as previously described (Le Guyader et al., 2008). The success of the microinjection was immediately checked by briefly observing bacterial (CFP or GFP) fluorescence in the otic cavity under a Leica Macrofluo microscope. During the subsequent time-lapse confocal fluorescence imaging session, only GFP-expressing bacteria were imaged, as repeated CFP confocal imaging using 405 nm laser illumination would be phototoxic to the embryos.

Parabiosis

Parabiotic embryos were generated as previously described (Demy et al., 2013) by fusing wt *Tg(mpx:GFP)^{i114}* embryos at the late blastula stage to stage-matched *mon^{NQ039}Tg(lysC:DsRed; gata1:DsRed)* embryos; mutant embryos were identified by the absence of circulating DsRed-positive erythroid cells.

Isolation of mouse BMDMs and 3D migration assays

Bone marrow cells were isolated from femurs and tibias of wt or *Trim33$^{fl/fl}$;Tg(Lyz:Cre)* mice (Ferri et al., 2015) and cultured in complete medium (RPMI 1640 with 10% fetal calf serum and 1% L-glutamine; Invitrogen) containing 20 ng/ml recombinant murine macrophage colony-stimulating factor (rmM-CSF; Immunotools) as described previously (Cougoule et al., 2010). After 7 days, adherent BMDMs were harvested and loaded at the surface of 3D extracellular matrices polymerized in transwell inserts (about 500 BMDMs/transwell) as described previously (Van Goethem et al., 2010). Fibrous collagen was used as a matrix triggering macrophage amoeboid migration, and Matrigel as a matrix triggering BMDM mesenchymal migration. 3D migration experiments were conducted for 48 h and the percentage of cell migration was monitored as previously described (Van Goethem et al., 2010).

Immunofluorescence microscopy on mouse macrophages

BMDMs (1.5×10^5) were seeded on glass coverslips for 24 h. Cells were fixed with paraformaldehyde (3.7%; Sigma) and permeabilized with Triton

X-100 (0.1%; Sigma), as previously described (Van Goethem et al., 2011; Cougoule et al., 2010) and stained with anti-vinculin antibody (clone HVin-1, dilution 1:300; Sigma) followed by FITC-conjugated goat anti-mouse-IgG antibody (1:500; Coger) and Texas Red-coupled phalloidin (Molecular Probes, Invitrogen). Slides were visualized with a Leica DM-RB fluorescence microscope.

Statistical analysis

To evaluate difference between means, a two-tailed unpaired *t*-test or an analysis of variance (ANOVA) followed by Bonferroni's multiple comparison test was used, when appropriate. Normal distributions were analysed with the Kolmogorov–Smirnov test. Non-Gaussian data were analysed with a Kruskal–Wallis test followed by Dunn's multiple comparison test. $P<0.05$ was considered statistically significant (***$P<0.001$; **$P<0.01$; *$P<0.05$). Statistical analyses and graphic representations were made using Prism software.

Acknowledgements

We thank Aude Parcelier and Paul-Henri Romeo (CEA, DSV, Fontenay-aux-Roses, France) for providing bones from *Trim33$^{fl/fl}$; Tg(Lyz:Cre)* mice and for suggesting to test the 3D mobility of their TRIM33-deficient macrophages *in vitro*. We are grateful to Milka Sarris (University of Cambridge, UK) and Elisa Gomez-Perdiguero (Institut Pasteur, Paris) for their critical reading of the manuscript.

Competing interests

The authors declare no competing or financial interests.

Author contributions

Conceptualization: D.L.D., M.T., V.I.C., I.M.-P., P.H.; Methodology: D.L.D., M.T., V.I.C., N.T.; Validation: D.L.D., M.T., V.I.C.; Formal analysis: D.L.D., V.I.C.; Investigation: D.L.D., M.T., M.L., V.I.C., M.R., E.M.; Resources: I.M.-P., N.T., P.H.; Writing - original draft: D.L.D., P.H.; Writing - review & editing: D.L.D., P.H.; Visualization: D.L.D., V.I.C.; Supervision: I.M.-P., P.H.; Project administration: P.H.; Funding acquisition: I.M.-P., P.H.

Funding

This work was supported by grants to P.H. from the European Commission through the Sixth Framework Programme 'ZF-Models' Integrated Project, from the Fondation pour la Recherche Médicale (FRM 2012 team) and from the Agence Nationale de la Recherche Laboratoire d'Excellence Revive (Investissement d'Avenir; ANR-10-LABX-73), and to I.M.-P. from the Fondation pour la Recherche Médicale (FRM 2011 team).

Supplementary information

Supplementary information available online at
http://jcs.biologists.org/lookup/doi/10.1242/jcs.203471.supplemental

References

Ashwell, K. (1989). Development of microglia in the albino rabbit retina. *J. Comp. Neurol.* **287**, 286-301.

Aucagne, R., Droin, N., Paggetti, J., Lagrange, B., Largeot, A., Hammann, A., Bataille, A., Martin, L., Yan, K.-P., Fenaux, P. et al. (2011). Transcription intermediary factor 1gamma is a tumor suppressor in mouse and human chronic myelomonocytic leukemia. *J. Clin. Invest.* **121**, 2361-2370.

Bai, X., Kim, J., Yang, Z., Jurynec, M. J., Akie, T. E., Lee, J., LeBlanc, J., Sessa, A., Jiang, H., DiBiase, A. et al. (2010). TIF1 gamma controls erythroid cell fate by regulating transcription elongation. *Cell* **142**, 133-143.

Cougoule, C., Le Cabec, V., Poincloux, R., Al Saati, T., Mege, J.-L., Tabouret, G., Lowell, C. A., Laviolette-Malirat, N. and Maridonneau-Parini, I. (2010). Three-dimensional migration of macrophages requires Hck for podosome organization and extracellular matrix proteolysis. *Blood* **115**, 1444-1452.

Cuadros, M. A., Coltey, P., Carmen Nieto, M. and Martin, C. (1992). Demonstration of a phagocytic cell system belonging to the hemopoietic lineage and originating from the yolk sac in the early avian embryo. *Development* **115**, 157-168.

Cuadros, M. A., Martin, C., Coltey, P., Almendros, A. and Navascués, J. (1993). First appearance, distribution, and origin of macrophages in the early development of the avian central nervous system. *J. Comp. Neurol.* **330**, 113-129.

Demy, D. L., Ranta, Z., Giorgi, J.-M., Gonzalez, M., Herbomel, P. and Kissa, K. (2013). Generating parabiotic zebrafish embryos for cell migration and homing studies. *Nat. Methods* **10**, 256-258.

Ferri, F., Parcelier, A., Petit, V., Gallouet, A.-S., Lewandowski, D., Dalloz, M., van den Heuvel, A., Kolovos, P., Soler, E., Squadrito, M. L. et al. (2015). TRIM33 switches off Ifnb1 gene transcription during the late phase of macrophage activation. *Nat. Commun.* **6**, 8900.

Hall, C. J., Flores, M. V., Oehlers, S. H., Sanderson, L. E., Lam, E. Y., Crosier, K. E. and Crosier, P. S. (2012). Infection-responsive expansion of the hematopoietic stem and progenitor cell compartment in zebrafish is dependent upon inducible nitric oxide. *Cell Stem Cell* **10**, 198-209.

He, W., Dorn, D. C., Erdjument-Bromage, H., Tempst, P., Moore, M. A. S. and Massagué, J. (2006). Hematopoiesis controlled by distinct TIF1gamma and Smad4 branches of the TGFbeta pathway. *Cell* **125**, 929-941.

Herbomel, P. and Levraud, J. P. (2005). Imaging early macrophage differentiation, migration, and behaviors in live zebrafish embryos. *Methods Mol. Med.* **105**, 199-214.

Herbomel, P., Thisse, B. and Thisse, C. (1999). Ontogeny and behaviour of early macrophages in the zebrafish embryo. *Development* **126**, 3735-3745.

Herbomel, P., Thisse, B. and Thisse, C. (2001). Zebrafish early macrophages colonize cephalic mesenchyme and developing brain, retina, and epidermis through a M-CSF receptor-dependent invasive process. *Dev. Biol.* **238**, 274-288.

Hesling, C., Fattet, L., Teyre, G., Jury, D., Gonzalo, P., Lopez, J., Vanbelle, C., Morel, A.-P., Gillet, G., Mikaelian, I. et al. (2011). Antagonistic regulation of EMT by TIF1gamma and Smad4 in mammary epithelial cells. *EMBO Rep.* **12**, 665-672.

Hesling, C., Lopez, J., Fattet, L., Gonzalo, P., Treilleux, I., Blanchard, D., Losson, R., Goffin, V., Pigat, N., Puisieux, A. et al. (2013). Tif1gamma is essential for the terminal differentiation of mammary alveolar epithelial cells and for lactation through SMAD4 inhibition. *Development* **140**, 167-175.

Hess, I. and Boehm, T. (2012). Intravital imaging of thymopoiesis reveals dynamic lympho-epithelial interactions. *Immunity* **36**, 298-309.

Hsu, K., Traver, D., Kutok, J. L., Hagen, A., Liu, T. X., Paw, B. H., Rhodes, J., Berman, J. N., Zon, L. I., Kanki, J. P. et al. (2004). The pu.1 promoter drives myeloid gene expression in zebrafish. *Blood* **104**, 1291-1297.

Kierdorf, K., Prinz, M., Geissmann, F. and Gomez Perdiguero, E. (2015). Development and function of tissue resident macrophages in mice. *Semin. Immunol.* **27**, 369-378.

Kurz, H. and Christ, B. (1998). Embryonic CNS macrophages and microglia do not stem from circulating, but from extravascular precursors. *Glia* **22**, 98-102.

Kusy, S., Gault, N., Ferri, F., Lewandowski, D., Barroca, V., Jaracz-Ros, A., Losson, R. and Romeo, P.-H. (2011). Adult hematopoiesis is regulated by TIF1gamma, a repressor of TAL1 and PU.1 transcriptional activity. *Cell Stem Cell* **8**, 412-425.

Le Guyader, D., Redd, M. J., Colucci-Guyon, E., Murayama, E., Kissa, K., Briolat, V., Mordelet, E., Zapata, A., Shinomiya, H. and and Herbomel, P. (2008). Origins and unconventional behavior of neutrophils in developing zebrafish. *Blood* **111**, 132-141.

Lelli, A., Gervais, A., Colin, C., Chéret, C., de Almodovar, C. R., Carmeliet, P., Krause, K.-H., Boillée, S. and Mallat, M. (2013). The NADPH oxidase Nox2 regulates VEGFR1/CSF-1R-mediated microglial chemotaxis and promotes early postnatal infiltration of phagocytes in the subventricular zone of the mouse cerebral cortex. *Glia* **61**, 1542-1555.

Monteiro, R., Pouget, C. and Patient, R. (2011). The gata1/pu.1 lineage fate paradigm varies between blood populations and is modulated by tif1 gamma. *EMBO J.* **30**, 1093-1103.

Mouchemore, K. A. and Pixley, F. J. (2012). CSF-1 signaling in macrophages: pleiotrophy through phosphotyrosine-based signaling pathways. *Crit. Rev. Clin. Lab. Sci.* **49**, 49-61.

Murayama, E., Kissa, K., Zapata, A., Mordelet, E., Briolat, V., Lin, H.-F., Handin, R. I. and Herbomel, P. (2006). Tracing hematopoietic precursor migration to successive hematopoietic organs during zebrafish development. *Immunity* **25**, 963-975.

Nguyen-Chi, M., Phan, Q. T., Gonzalez, C., Dubremetz, J.-F., Levraud, J.-P. and Lutfalla, G. (2014). Transient infection of the zebrafish notochord with E. coli induces chronic inflammation. *Dis. Model. Mech.* **7**, 871-882.

Palha, N., Guivel-Benhassine, F., Briolat, V., Lutfalla, G., Sourisseau, M., Ellett, F., Wang, C.-H., Lieschke, G. J., Herbomel, P., Schwartz, O. et al. (2013). Real-time whole-body visualization of chikungunya virus infection and host interferon response in zebrafish. *PLoS Pathog.* **9**, e1003619.

Quere, R., Saint-Paul, L., Carmignac, V., Martin, R. Z., Chretien, M.-L., Largeot, A., Hammann, A., Pais de Barros, J.-P., Bastie, J.-N. and and Delva, L. (2014). Tif1gamma regulates the TGF-beta1 receptor and promotes physiological aging of hematopoietic stem cells. *Proc. Natl. Acad. Sci. USA* **111**, 10592-10597.

Ransom, D. G., Bahary, N., Niss, K., Traver, D., Burns, C., Trede, N. S., Paffett-Lugassy, N., Saganic, W. J., Lim, C. A., Hersey, C. et al. (2004). The zebrafish moonshine gene encodes transcriptional intermediary factor 1gamma, an essential regulator of hematopoiesis. *PLoS Biol.* **2**, e237.

Renshaw, S. A., Loynes, C. A., Trushell, D. M. I., Elworthy, S., Ingham, P. W. and Whyte, M. K. B. (2006). A transgenic zebrafish model of neutrophilic inflammation. *Blood* **108**, 3976-3978.

Rombough, P. (2002). Gills are needed for ionoregulation before they are needed for O(2) uptake in developing zebrafish, Danio rerio. *J. Exp. Biol.* **205**, 1787-1794.

Sorokin, S. P., Hoyt, R. F., Jr, Blunt, D. G. and McNelly, N. A. (1992). Macrophage development: II. Early ontogeny of macrophage populations in brain, liver, and lungs of rat embryos as revealed by a lectin marker. *Anat. Rec.* **232**, 527-550.

Takahashi, K., Yamamura, F. and Naito, M. (1989). Differentiation, maturation, and proliferation of macrophages in the mouse yolk sac: a light-microscopic, enzyme-cytochemical, immunohistochemical, and ultrastructural study. *J. Leukoc. Biol.* **45**, 87-96.

Takahashi, K., Naito, M. and Takeya, M. (1996). Development and heterogeneity of macrophages and their related cells through their differentiation pathways. *Pathol. Int.* **46**, 473-485.
Thisse, C. and Thisse, B. (2008). High-resolution in situ hybridization to whole-mount zebrafish embryos. *Nat. Protoc.* **3**, 59-69.
Traver, D., Paw, B. H., Poss, K. D., Penberthy, W. T., Lin, S. and Zon, L. I. (2003). Transplantation and *in vivo* imaging of multilineage engraftment in zebrafish bloodless mutants. *Nat. Immunol.* **4**, 1238-1246.
van Eeden, F. J. M., Granato, M., Odenthal, J. and Haffter, P. (1999). Developmental mutant screens in the zebrafish. *Methods Cell Biol.* **60**, 21-41.
Van Goethem, E., Poincloux, R., Gauffre, F., Maridonneau-Parini, I. and Le Cabec, V. (2010). Matrix architecture dictates three-dimensional migration modes of human macrophages: differential involvement of proteases and podosome-like structures. *J. Immunol.* **184**, 1049-1061.
Van Goethem, E., Guiet, R., Balor, S., Charrière, G. M., Poincloux, R., Labrousse, A., Maridonneau-Parini, I. and Le Cabec, V. (2011). Macrophage podosomes go 3D. *Eur. J. Cell Biol.* **90**, 224-236.
van Ham, T. J., Mapes, J., Kokel, D. and Peterson, R. T. (2010). Live imaging of apoptotic cells in zebrafish. *FASEB J.* **24**, 4336-4342.
Xi, Q., Wang, Z., Zaromytidou, A.-I., Zhang, X. H.-F., Chow-Tsang, L.-F., Liu, J. X., Kim, H., Barlas, A., Manova-Todorova, K., Kaartinen, V. et al. (2011). A poised chromatin platform for TGF-beta access to master regulators. *Cell* **147**, 1511-1524.
Xu, J., Wang, T., Wu, Y., Jin, W. and Wen, Z. (2016). Microglia colonization of developing zebrafish midbrain is promoted by apoptotic neuron and lysophosphatidylcholine. *Dev. Cell* **38**, 214-222.
Yoo, S. K., Starnes, T. W., Deng, Q. and Huttenlocher, A. (2011). Lyn is a redox sensor that mediates leukocyte wound attraction in vivo. *Nature* **480**, 109-112.